Word learning is mediated by the left arcuate fasciculus

Diana López-Barroso[a,b,1], Marco Catani[c], Pablo Ripollés[a,b], Flavio Dell'Acqua[c,d,e], Antoni Rodríguez-Fornells[a,b,f], and Ruth de Diego-Balaguer[a,b,f]

[a]Cognition and Brain Plasticity Group, Bellvitge Biomedical Research Institute, L'Hospitalet de Llobregat, 08097 Barcelona, Spain; [b]Department of Basic Psychology, Campus Bellvitge, University of Barcelona, L'Hospitalet de Llobregat, 08097 Barcelona, Spain; [c]Natbrainlab, Department of Forensic and Neurodevelopmental Sciences, Institute of Psychiatry, and [d]Department of Neuroimaging, Institute of Psychiatry, King's College London, London SE5 8AF, United Kingdom; [e]National Institute for Health Research Biomedical Research Centre for Mental Health at South London and Maudsley National Health Service Foundation Trust and King's College London, Institute of Psychiatry, London SE5 8AF, United Kingdom; and [f]Institució Catalana de Recerca i Estudis Avançats, 08010 Barcelona, Spain

Edited* by Mortimer Mishkin, National Institute for Mental Health, Bethesda, MD, and approved July 5, 2013 (received for review January 26, 2013)

Human language requires constant learning of new words, leading to the acquisition of an average vocabulary of more than 30,000 words in adult life. The ability to learn new words is highly variable and may rely on the integration between auditory and motor information. Here, we combined diffusion imaging tractography and functional MRI to study whether the strength of anatomical and functional connectivity between auditory and motor language networks is associated with word learning ability. Our results showed that performance in word learning correlates with microstructural properties and strength of functional connectivity of the direct connections between Broca's and Wernicke's territories in the left hemisphere. This study suggests that our ability to learn new words relies on an efficient and fast communication between temporal and frontal areas. The absence of these connections in other animals may explain the unique ability of learning words in humans.

white matter | dorsal stream | ventral stream | diffusion tensor imaging

Language is a unique human ability that has been suggested to depend on the evolution of direct connections between the temporal and frontal cortex for the integration of auditory and motor representation of words (1). Auditory-motor integration, involving the mapping of sound into articulation, has been proposed to be important not only for auditory perception (2) and speech processing (3, 4), but also for learning new words (1, 3, 5). The auditory-motor integration theory of speech is based in part on the observation that patients with lesions affecting the arcuate fasciculus (AF) connecting temporal and frontal cortices, are impaired not only in phonological and word repetition but also in verbal short-term memory tasks (6, 7). Moreover, stimulation of the premotor cortex with repetitive transcranial magnetic stimulation disrupts the capacity to discriminate between phonemes (8). Similarly, learning new words is impaired if participants are engaged in the articulation of irrelevant sounds while they try to learn new ones (9). These studies are supportive of a link between auditory and motor processes in word learning.

Auditory and motor areas communicate directly through the AF, a pathway that shows a progressively high degree of complexity along the phylogenetic scale (10–13). Axonal tracing studies in monkey have shown that the AF connects to more dorsal regions of the temporo-parietal cortex (11, 14), whereas diffusion tensor imaging (DTI) studies in humans show a greater level of connectivity to auditory regions of the temporal lobe (10, 12). On the basis of these anatomical differences between human and other species, it has been suggested that the evolutionary expansion of auditory-motor connections allowed humans to develop a system for auditory working memory critical for learning complex phonological sequences (1, 15). There is, however, no experimental evidence so far that links the anatomy of the AF with word learning ability.

In the present study, we aimed to seek direct evidence of the role of the AF in auditory-motor integration and word learning. For that purpose, we explored the pattern of structural and functional connectivity between auditory and motor areas in both hemispheres as assessed by DTI-tractography and functional MRI (fMRI) as participants were learning words from fluent speech (Fig. 1*A*).

In our study we have used a recently described model of the AF (10, 16) in which communication between temporal and frontal language areas is mediated by two parallel networks: a direct pathway (i.e., the long segment of the AF), which connects the posterior part of both superior [Brodmann area (BA) 22] and middle (BA 37) temporal gyrus (Wernicke's territory) with the inferior frontal gyrus (BA 44 and 45), the middle frontal gyrus (BA 46) and the premotor cortex (BA 6) (Broca's territory); an indirect pathway composed of an anterior segment connecting Broca's territory with the inferior parietal cortex (BA 39 and 40) (Geschwind's territory) and a posterior segment connecting Geschwind's with Wernicke's territories (Fig. 1*B*). Our primary hypothesis was that word learning ability correlates with structural and functional connectivity of tracts directly connecting auditory and motor areas (i.e., long segment). Alternatively, previous evidence suggests that a ventral pathway running through the extreme capsule also connects the language areas (17–19). This path connects the inferior frontal gyrus (BA 45/47) with the superior temporal gyrus (BA 22), inferior parietal (BA 39) and occipital cortices (BA 17, 18, and 19) (12, 18, 20), and it has been claimed to be important for spoken-word recognition (21). During auditory word learning, the ventral pathway may allow the categorization of words as familiar once they have been learned, a point that could be also crucial for successful learning. This pathway corresponds to the inferior fronto-occipital fasciculus (IFOF), which was dissected bilaterally (Fig. 1*B* and Fig. S1).

Results

Virtual dissections of the AF and the IFOF were performed in 21 right-handed healthy subjects (mean age = 25.6 ± 3.9 y, nine females) and surrogate measures of volume (i.e., number of streamlines) and microstructural properties of fibers possibly related to the degree of myelination, axonal architecture, and diameter [i.e., fractional anisotropy (FA) and radial diffusivity

Author contributions: D.L.-B., M.C., A.R.-F., and R.d.D.-B. designed the study; D.L.-B. and R.d.D.-B. performed the research; D.L.-B., M.C., P.R., F.D., and R.d.D.-B. analyzed the data; and D.L.-B., M.C., P.R., F.D., A.R.-F., and R.d.D.-B. wrote the paper.

The authors declare no conflict of interest.

*This Direct Submission article had a prearranged editor.

[1]To whom correspondence should be addressed. E-mail: dlopezbarroso@gmail.com.

This article contains supporting information online at www.pnas.org/lookup/suppl/doi:10.1073/pnas.1301696110/-/DCSupplemental.

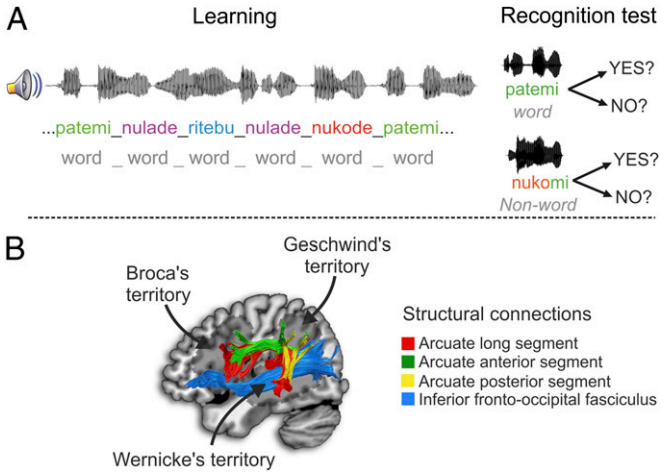

Fig. 1. Task and methods used in the study. (*A*) Schematic illustration of the word learning task consisting of a learning phase and a recognition test. The learning phase consisted in the auditory presentation of an artificial language stream composed by trisyllabic words separated by brief pauses. The test phase consisted in the presentation of isolated words ("words" or "nonwords") and participants were required to recognize each one as correct or incorrect based in the previously heard artificial language. (*B*) Example of tractography reconstruction of language pathways in the left hemisphere for one of the subjects rendered onto the Montreal Neurological Institute (MNI) template.

(RD)] were measured along the reconstructed streamlines (22) (see *Materials and Methods*). The analysis was performed separately for the three segments of the AF (Fig. 1*B* and *SI Materials and Methods*) and the IFOF (Fig. 1*B*, Fig. S1, and *SI Materials and Methods*) in both left and right hemispheres.

The word learning task involved two phases (Fig. 1*A* and *Materials and Methods*). In the learning phase participants were asked to memorize artificially created words composed of three syllables presented in the form of a fluent speech stream (23). The words were novel to the participants and had no semantic content. The learning task was performed in the MRI scan during the fMRI experiment. Immediately after the learning phase, participants were behaviorally tested and asked to recognize auditory presented words (recognition phase) (see *Materials and Methods* for further details). Word learning performances were measured using hit rates taking into account false alarms, calculating the *d*-prime (d') index (24), which reflects individual's ability to discriminate words presented in the artificial language from nonpresented words (nonwords) (*SI Materials and Methods*). One-sample *t* test against $d' = 0$ (no discrimination) showed significant learning: $t(24) = 2.74$, $P < 0.01$.

Relationship Between Word Learning Performance and Tract Properties of the AF and IFOF. After Bonferroni's correction for multiple comparisons, a statistically significant negative correlation was found between word learning performance and radial diffusivity ($r = -0.6$; $P < 0.005$) in the left long segment (Fig. 2 and Table S1). Correlations with the anterior and posterior segments were not statistically significant (Fig. 2 and Table S1). There were no significant correlations with all three segments in the right hemisphere (Fig. 2 and Table S1). These findings suggest that microstructural properties of the dorsal direct connections between temporal and frontal language regions in the left hemisphere correlate with individual abilities to learn new words. In addition, a lateralization index was calculated by counting the number of reconstructed streamlines within each segment of the AF for each hemisphere (*Materials and Methods*, *SI Materials and Methods*, and Fig. S2). In agreement with previous reports (16), the long segment was left lateralized, the anterior segment right lateralized, and the posterior segment symmetrically distributed (Fig. S2 and Table S2). No significant correlation was observed between the lateralization of each segment of the AF and learning performance (Table S2).

No statistically significant correlations were found between any of the DTI-derived measures and word learning scores for the IFOF of either hemisphere (Table S3). Analysis of the lateralization indices showed a symmetrical distribution for the number of streamlines of the IFOF and a left lateralization of its FA (Fig. S2 and Table S2). No significant correlation was found between the lateralization index of the IFOF and learning performance (Table S2).

Relationship Between Word Learning Performance and Functional Connectivity. Functional connectivity analysis was performed using the temporal correlation of the blood oxygen level-dependent (BOLD) response between the three regions of the perisylvian network connected by the direct and indirect segments of the AF on both hemispheres (*Materials and Methods*). Results showed that individual variations in the strength of the functional connectivity between the left temporal (Wernicke's territory) and frontal (Broca's territory) areas correlated with word learning performance ($r = 0.42$, $P < 0.036$) (Fig. 3*A*). The strength of connectivity between right frontal and temporal regions or

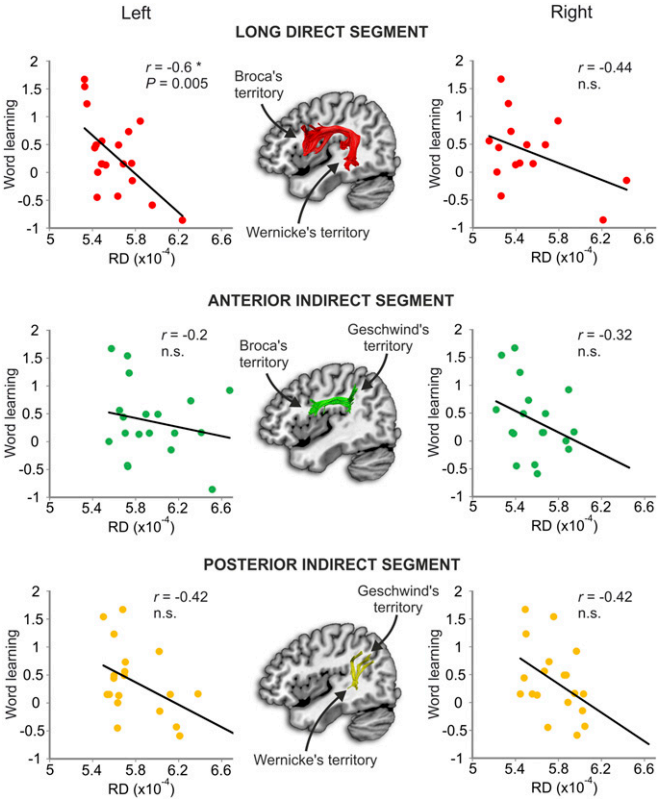

Fig. 2. Link between the microstructure of the AF and word learning performance. The scatter plots show the correlations between word learning scores (d') and RD in the long, anterior, and posterior segments of the AF for the left and right hemispheres. The index of correlation and the *P* value are provided on each plot box. An asterisk indicates the significant correlation ($P < 0.0062$). Nonsignificant correlations are marked as "n.s." $d' = 0$ designates no learning. Positive values reflect that participants discriminate words and nonwords accurately. Negative values indicate discrimination is achieved but individuals segmented incorrectly, classifying nonwords as words of the artificial language.

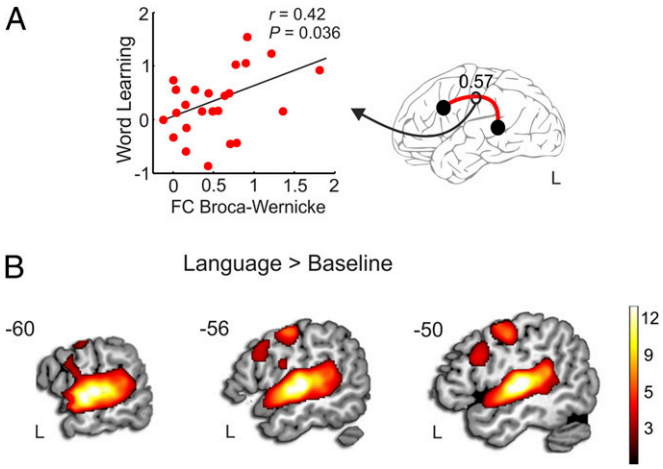

Fig. 3. fMRI analysis. (*A*) Scatter plot showing the correlation between word learning (*d′*) and the amount of functional connectivity between Broca's and Wernicke's territories in the left hemisphere during the word-learning task. Correlation index and the *P* value are provided on the plot box. The averaged functional connectivity (0.57) was significantly different from zero ($P < 0.001$). (*B*) Language versus baseline contrast in sagittal views superimposed on the MNI template ($P < 0.05$ FDR-corrected). Only activations in the left hemisphere are shown in the figure. See Table S5 for peak activation coordinates.

between the regions connected by the indirect segments in both hemispheres was not significantly correlated with performance (all $P > 0.1$). In addition, laterality analysis of functional connectivity between regions connected by each AF segment was also calculated (*Materials and Methods* and *SI Materials and Methods*). There was no significant correlation between the functional lateralization indices and word learning performance (all $P > 0.09$) (Table S4).

Relationship Between Structural and Functional Connectivity. Tract-specific measurements of single segments and strength of the functional connectivity between perisylvian areas were used to analyze possible correlations between anatomical and functional connectivity. We found no significant correlations between diffusion parameters and measures of functional connectivity (all $P > 0.1$).

Discussion

The present study combines tractography and fMRI in direct support of the role of the AF in word learning. Our main results suggest that both structural and functional measures of connectivity between temporal and frontal language territories in the left hemisphere predict word learning abilities. The fact that correlations for the indirect pathways were not significant suggests that the direct connections are crucial for auditory-motor integration in word learning. The direct connections of the AF could mediate fast interaction between auditory and motor areas in the left hemisphere, thus facilitating those feed-forward and feed-back exchanges of information that are required to phoneme categorization (25) as well as to create the motor codes of the new phonological sequences (4, 5). Moreover, this sensory-motor circuit may provide the substrate for articulatory-based processes that allow keeping information active during working memory (26, 27).

In addition, word learning did not correlate with any of the microstructural measures of the ventral IFOF, indicating that auditory-motor integration through the dorsal pathway is a critical function at these earliest stages of language learning. The ventral pathway may nevertheless play a greater role at later stages of learning, when auditory representations of learned words are consolidated by taking into account invariance properties after multiple encounters (28), as well as once conceptual representations have been attached to the new words learned (29). Furthermore it is possible that word learning through the ventral pathway could be mediated by other tracts that were not included in our analysis (e.g., the uncinate fasciculus) (30).

A basic aspect of human language is its left-side lateralization (31). In our study, the correlation between language learning and the direct segment of the AF was exclusively found in the left hemisphere. This left lateralized relation was not relative to the characteristics of the right AF because lateralization indexes showed no correlation with word learning performance. Previous work found correlations between verbal memory for known words and the AF bilaterally (16). Compared with our study, the previous study used a task that required a semantic recall strategy for real words, which is known to be associated with bilateral activation of fronto-temporal networks (32). In contrast, no semantic component was present in our task, which was designed to have a purely phonological component and therefore to test a more simple auditory-motor integration strategy.

The present findings add unique insights into the relationship between brain morphology and language proficiency, previously explored by neuroimaging studies looking at the anatomy of single cortical regions. For example, the gray matter density of Broca's area has been found to correlate with the level of language proficiency (33) and the number of years of phonetic training in expert phoneticians (34). Similarly, white matter density in left parietal regions (35, 36) and the superior temporal gyrus (36) predicts speech sound learning. Interestingly, a recent study has shown that changes in the cortical thickness of Broca's area and left superior temporal gyrus can occur even only after 3 mo of intensive language training (37). On the other hand, the aforementioned findings, together with our results, contrast with retrospective studies showing an association between gray matter density in the posterior parietal cortex and vocabulary size of the first (38) and second language (39). These findings suggest that learning and storing new words rely on different anatomical structures, the former on temporal-frontal regions, the latter on inferior parietal areas.

The correlation we found with structural measures of connectivity suggests that radial diffusivity is a sensitive index of white matter microstructural features underlying efficient cognitive processing. Several factors, like axon diameter, fiber packing density, number of axons, fiber cohesiveness, and myelin thickness may contribute to radial diffusivity signal (22). Importantly, thicker myelin and larger diameter axons are correlated with increased conduction of action potentials through long association fibers (40). A decrease in radial diffusivity [i.e., the average of the diffusivities along the two minor axes of the tensor model (41)], is likely to reflect increased myelination or increased axonal diameter (42). Hence, the correlation reported in our study suggests that a possible explanation for the inter-individual variability in word learning is a result of differences in the anatomy of direct connections between left auditory and motor areas. One could speculate that fibers with larger axons or greater myelination facilitate faster conduction of impulses, leading to better synchronization and information transfer between distant regions.

In addition, our results show that functional connectivity is an independent predictor of word learning performance. Several studies have focused on the physiological processes underpinning the fluctuations that are commonly observed in the BOLD response as measured by fMRI (43–45). The BOLD signal is sensitive to changes in the oxygenation of the blood in a given area, which is associated to its increased neuronal activation (46). In relation to neural activity, BOLD response fluctuations reflect more the input and local processing of an area rather than its output (i.e., spiking activity) (45). Conversely, DTI is more

sensitive to differences in white matter microstructure, such as axonal density, myelination, or fiber diameter (22). These microstructural properties of fibers are likely to facilitate a faster signal conduction but they may not be related to integrative processes performed at the cortical level (47, 48). Indeed, our results suggest that, although both functional and anatomical measures of connectivity are correlated to language-learning performances, a correlation between them should not be assumed.

Finally, the AF, taken as a possible anatomical substrate of auditory-motor integration, might represent a key step for language development. Comparative studies indicate that apes and monkeys have homologs for Broca's and Wernicke's areas in terms of gray matter (49, 50) connected by a dorsal and a ventral pathway (49). However, the trajectory of the AF is different between species. Middle and inferior temporal gyri terminations from the inferior frontal gyrus are more prominent in humans than in macaques and chimpanzees (12, 13, 49). In addition, the AF appears to show a greater modification in human evolution than the ventral fiber system of the extreme capsule (51). Indeed, although humans and chimpanzees show a dominant connection between Broca's and Wernicke's territories through the AF, macaques show a predominant connection through the ventral pathway (13). This latter path, involved in auditory object identification, is the one processing calls and vocalizations in these lower species (51). Interestingly, monkeys, which have a smaller AF compared to humans (11, 14), are able to perform complex tactile and visual memory tests but these skills are lost in the auditory modality (52). These findings suggest that the ability to integrate auditory-motor information confers some advantages in the manipulation of the representation of acoustic stimuli, thus allowing its storage in the long-term memory.

Ontogenetically, the AF develops slower than other associative pathways, including the ventral pathway (19). The AF's terminations connecting with Broca's area show progressive development during childhood, still under development at the age of 7 y (53, 54). However, the connections with premotor cortex, those responsible to auditory-motor integration, can be tracked in newborns (19, 54), suggesting a role in early language acquisition. Very early prelinguistic damage to the AF (55) induces delayed expressive language development and residual language difficulties remain even when within-normal levels of expressive language are reached later on through the available connectivity of the ventral pathway. Similar lesions after the age of 5 y (56) lead to preserved oral language, although with poor performance in nonword repetition, verbal working memory, and reading. In healthy adults, the use of articulatory suppression to block the use of the dorsal pathway interferes with word learning as well, and performance under this condition correlates with individual differences in the microstructural properties of the ventral pathway (9). Taken together, the above studies indicate that lesions to the AF induce language-learning difficulties. Even when the ventral system can compensate for language learning, optimal performance cannot be reached after complete damage of the AF.

It is noteworthy that despite the differences in terminology, each of the three segments composing the AF in the model adopted in the present study have some correspondence to what has been previously described in the monkey brain using axonal tracing (11, 12). The anterior segment corresponds to the third branch of the superior longitudinal fasciculus (SLF III); the long segment corresponds to the arcuate *sensu strictu*; and the posterior segment includes fibres of the middle longitudinal fasciculus. In this study we have used DTI instead of more advanced methods, such as high angular resolution diffusion imaging or diffusion spectrum imaging. These methods lead to greater number of false-positive streamlines in the AF reconstruction that need to be anatomically validated (57). Thus, for AF, tractography based on DTI still remains a more conservative and reliable method (for a more in depth critique, see ref. 55, 58).

In conclusion, the present results support the idea that the direct segment of the AF is crucial for word learning, most probably because of its relevance to auditory-motor integration. This study also sheds light on the origin of the large individual variability observed when learning a new language and gives support to the idea that anatomical brain connectivity constrains the nature of the information processed across brain regions (59). The differences between humans and nonhuman primates in language learning might be related to the evolution of the AF, a pathway that has been shown to be structurally different in nonhuman primates, and that facilitates processing and manipulation of complex auditory information in humans.

Materials and Methods

Participants. Twenty-seven adult participants (mean age = 24.7 ± 4.6, 12 women) were recruited for the experiment. Participants were native Spanish speakers with no history of auditory problems. All participants in this study were classified as right-handed after completing the Edinburgh Handedness Inventory (mean 80.4 ± 20.4) (60). The ethical committee of the University of Barcelona approved the protocol and written consent was obtained from all participants. Participants were paid for their participation. Six participants were removed for the tractography analysis because of MRI acquisition problems and two participants were removed from the behavioral correlations because no behavioral data were obtained from them. The final sample resulted in 20 subjects for the behavioral-tractography correlations, 25 for the behavioral-functional connectivity correlation, and 21 for the tractography-functional correlations.

Language Learning Task Design. An artificial language-learning task was administered during fMRI scanning (Fig. 1*A*) through two runs. Eight different languages were built with each participant listening to two different languages. Languages were counterbalanced between subjects and were built by creating words composed of three syllables. Words were synthesized using the MBROLA speech synthesizer software (61) concatenating diphones at 16 kHz from the Spanish male database (http://tcts.fpms.ac.be/synthesis/). Languages were composed by nine different novel words built following Spanish phonotactic constrains. Each word had a 696-ms duration and brief pauses of 25 ms were inserted between them to introduce a prosodic cue marking words boundaries (62). Words were presented in pseudorandom order (i.e., the same word was not repeated in succession) and in the form of a fluent speech stream. The material was similar to the one used in de Diego-Balaguer et al. (23).

The task involved a learning phase and a test phase (Fig. 1*A*). The learning phase consisted of four active blocks lasting 30 s, and included 42 word presentations each. Active blocks were alternated with resting blocks of 20 s duration where participants were asked to simply fixate their gaze on a cross that remained in the middle of the screen.

Participants were told that they would hear a nonsense language and that their task was to pay attention to it because they would be asked to recognize words of this language after listening. Immediately after the learning phase, participants were behaviorally tested (recognition phase). Isolated words were presented auditorily and participants were required to judge whether each word had appeared in the previously learned language stream. Test items could be previously presented words, or nonwords formed with the same three syllables but in an incorrect order (Fig. 1*A*). Each test item appeared three times in each recognition phase. Responses were recorded using an MR-compatible response box containing two response keys (forefinger and middle-finger). Participants were required to press the left or right button, respectively, to judge whether the item was a word presented before or not. The experiment was run using the Presentation Software (www.neurobs.com). Stimuli were played through MR-compatible headphones.

MRI Acquisition. Images were acquired on a 3T MRI scanner (Siemens Magnetom Trio) with 40-mT/m gradients, using an acquisition sequence fully optimized for DT-MRI of white matter, with the following parameters: voxel size of 2.0 × 2.0 × 2.0 mm, matrix 128 × 128, 64 slices with 2-mm-thick and no gap, NEX 1, TE 88 ms, b-value 1,000 s/mm^2, eight runs of 12 diffusion-weighted directions and seven nondiffusion-weighted volumes, using a spin-echo echo-planar imaging (EPI) sequence coverage of the whole head. DTI images were acquired before the fMRI sequence. High-resolution structural

images [T1-weighted sequence: slice thickness = 1 mm; no gap; number of slices = 240; repetition time (TR) = 2,300 ms; echo time (TE) = 3 ms; matrix = 256 × 256; field-of-view (FOV) = 244 mm] were also acquired. Subsequently, functional images were obtained by using a single-shot T2*-weighted gradient-echo EPI sequence (slice thickness = 4 mm; no gap; number of slices = 32, order of acquisition interleaved; TR = 2,000 ms; TE = 29 ms; flip angle = 80°; matrix = 128 × 128; FOV = 240 mm).

DTI-MRI Tractography. ***Preprocessing of DTI data.*** Diffusion data were processed using Explore DTI (www.exploredti.com). Data were first preprocessed for eddy current distortions and head motion. For each subject the b-matrix was then reoriented to provide a more accurate estimate of diffusion tensor orientations (63). Remaining artifacts caused by subject motion and cardiac pulsation were excluded from the analysis using RESTORE (64) to reject and correct outliers from diffusion-weighted imaging data. Diffusion tensor was estimated using a nonlinear least-squares approach (65) and FA and RD maps were calculated. Whole-brain tractography was performed using a b-spline interpolation of the diffusion tensor field and Euler integration to propagate streamlines following the directions of the principal eigenvector with a step size of 0.5 mm (66). Tractography was started in all brain voxels with FA > 0.2. Tractography was stopped where FA < 0.2 or when the angle between two consecutive tractography steps was larger than 35°. This whole-brain approach ensures that tractography reconstruction is less dependent on the regions of interest (ROI) delineation. Finally, tractography data and diffusion tensor maps were exported into Trackvis (67) for manual dissection of the tracts.

Tractography dissections. Virtual dissections of the AF and the IFOF were carried out as described in previous studies (10, 16, 68) (see *SI Materials and Methods* for further details). Dissections were performed for each subject in the native space and in both hemispheres. The color fiber-orientation maps were resliced in axial, coronal, and sagittal planes and displayed in conjunction with tractography results to allow an approximation to the neuroanatomical location of the tract reconstructions. Because brain regions may have significant interindividual differences, ROIs were manually defined (i.e., the dissector placed the ROI according to individual anatomical landmarks, rather than coordinates or atlas-based constraints that may not apply to each single subject). The approach does not constrain tracts to start and end within the defined regions (*SI Materials and Methods*).

Tracts-specific measurements. The number of streamlines (Ns), FA, and RD were extracted and averaged along the entire segmented tract (22). Ns is considered as a surrogate measure of tract volume; FA is considered as a measure linked to axonal architecture and myelination; RD describes miscroscopic water movements perpendicular to the fibers (69) and has been postulated to reflect myelin content along the axon. Demyelination (42) and severe tissue injury (70) have been associated with increased RD.

Statistical analysis. The statistical analysis was performed using the SPSS software. Pearson's correlation analysis was performed between the learning performance (d' index) and the DTI measures (Ns, FA, RD) along each segment (long, anterior, posterior) of the AF as well as for the IFOF pathway from both hemispheres (Fig. 1*B*). Correlations were considered significant at $P < 0.0062$ after Bonferroni's correction for multiple comparisons. Values that were greater than two SDs from the mean were considered outliers and were removed from the analysis (see Tables S1 and S3 for the final sample of each correlation analysis). A lateralization index was calculated for the Ns and FA according to the following formula: [(left) − (right)]/[(left) + (right)] (*SI Materials and Methods*) (16).

fMRI. ***Preprocessing.*** Data were preprocessed using Statistical Parameter Mapping software (SPM8, Wellcome Department of Imaging Neuroscience, University College, London, United Kingdom, www.fil.ion.ucl.ac.uk/spm). Preprocessing included realignment, coregistration between the mean functional and the structural T1, segmentation, normalization, and smoothing with an 8-mm FWHM Gaussian kernel. Normalization was performed using DARTEL (71).

Statistical analysis was based on a least-squares estimation using the general linear model by convolving a box-car regressor waveform with a canonical hemodynamic response function. Two main conditions of interest were modeled, language and rest. Parameters from head movement, obtained from realignment, were also included in the model. Main effects for each condition were calculated and the contrast of interest (language vs. rest) was estimated for each participant. A second level RFX analysis was performed by using a one-sample *t* test on the main contrast derived from the single subject data. Results are shown at a $P < 0.05$ false-discovery rate (FDR)-corrected (Fig. 3*B* and Table S5).

Functional connectivity (fcMRI) and statistical analysis. Three ROIs were manually defined based on the anatomical gyri around the territories connected by the direct and the indirect segments of the AF (*SI Materials and Methods* and Fig. S3). The predominant tissue in each of the ROIs defined for functional connectivity analyses was gray matter (around 65%) (see *SI Materials and Methods* and Table S6 for further details). First-level subject-specific language vs. rest contrasts were masked with the defined ROIs, and for each subject, the peak coordinate within each ROI was selected. Eight-millimeter radius 3D-seeds were placed at the selected coordinates and mean voxel time-course series was extracted. These mean time courses were low-pass filtered and had the linear trend removed. MATLAB toolbox for functional connectivity (72) includes a function that calculates the relationship between two regions, after taking into account the influence of any other area. This toolbox was used to calculate correlations between the time series of each pair of territories. Finally, this correlation was transformed to a normal distribution using Fisher's *z* transform (73).

Functional-behavioral correlations were performed for the areas in the frontal, temporal, and parietal cortices that the direct and the indirect segments of the AF connect (Broca, Wernicke, and Geschwind territories, respectively). Each subject's *z*-transformed left and right correlations were regressed with behavioral performance (d' scores).

ACKNOWLEDGMENTS. We thank Virginia Penhune for her helpful discussions on the results. The present project was funded by the FP7 ERC StG_313841 TuningLang (to R.d.D.-B.); the Spanish Government Ministry of Economy and Competitiveness Grants PSI2011-23624 (to R.d.D.-B.) and PSI2011-29219 (to A.R.-F.); predoctoral Grant 2010FI_B1 00169 from the Catalan government (to D.L.-B.); predoctoral Formación de Profesorado Universitario Grant AP2010-4179 from the Spanish Government (to P.R.); and in part by Guy's and St Thomas' Charity and the Biomedical Research Centre for Mental Health at South London and Maudsley National Health Service Foundation Trust and Institute of Psychiatry, King's College London.

1. Schulze K, Vargha-Khadem F, Mishkin M (2012) Test of a motor theory of long-term auditory memory. *Proc Natl Acad Sci USA* 109(18):7121–7125.
2. Liberman AM, Mattingly IG (1985) The motor theory of speech perception revised. *Cognition* 21(1):1–36.
3. Hickok G, Poeppel D (2007) The cortical organization of speech processing. *Nat Rev Neurosci* 8(5):393–402.
4. Rauschecker JP, Scott SK (2009) Maps and streams in the auditory cortex: Nonhuman primates illuminate human speech processing. *Nat Neurosci* 12(6):718–724.
5. Rodríguez-Fornells A, Cunillera T, Mestres-Missé A, de Diego-Balaguer R (2009) Neurophysiological mechanisms involved in language learning in adults. *Philos Trans R Soc Lond B Biol Sci* 364(1536):3711–3735.
6. Benson DF, et al. (1973) Conduction aphasia. A clinicopathological study. *Arch Neurol* 28(5):339–346.
7. Damasio H, Damasio AR (1980) The anatomical basis of conduction aphasia. *Brain* 103(2):337–350.
8. Meister IG, Wilson SM, Deblieck C, Wu AD, Iacoboni M (2007) The essential role of premotor cortex in speech perception. *Curr Biol* 17(19):1692–1696.
9. Lopez-Barroso D, et al. (2011) Language learning under working memory constraints correlates with microstructural differences in the ventral language pathway. *Cereb Cortex* 21(12):2742–2750.
10. Catani M, Jones DK, ffytche DH (2005) Perisylvian language networks of the human brain. *Ann Neurol* 57(1):8–16.
11. Schmahmann JD, et al. (2007) Association fibre pathways of the brain: Parallel observations from diffusion spectrum imaging and autoradiography. *Brain* 130(Pt 3):630–653.
12. Thiebaut de Schotten M, Dell'Acqua F, Valabregue R, Catani M (2012) Monkey to human comparative anatomy of the frontal lobe association tracts. *Cortex* 48(1):82–96.
13. Rilling JK, et al. (2008) The evolution of the arcuate fasciculus revealed with comparative DTI. *Nat Neurosci* 11(4):426–428.
14. Petrides M, Pandya DN (1984) Projections to the frontal cortex from the posterior parietal region in the rhesus monkey. *J Comp Neurol* 228(1):105–116.
15. Aboitiz F (2012) Gestures, vocalizations, and memory in language origins. *Front Evol Neurosci* 4:2.
16. Catani M, et al. (2007) Symmetries in human brain language pathways correlate with verbal recall. *Proc Natl Acad Sci USA* 104(43):17163–17168.
17. Saur D, et al. (2008) Ventral and dorsal pathways for language. *Proc Natl Acad Sci USA* 105(46):18035–18040.
18. Martino J, Brogna C, Robles SG, Vergani F, Duffau H (2010) Anatomic dissection of the inferior fronto-occipital fasciculus revisited in the lights of brain stimulation data. *Cortex* 46(5):691–699.
19. Perani D, et al. (2011) Neural language networks at birth. *Proc Natl Acad Sci USA* 108(38):16056–16061.
20. Catani M, Howard RJ, Pajevic S, Jones DK (2002) Virtual in vivo interactive dissection of white matter fasciculi in the human brain. *Neuroimage* 17(1):77–94.
21. DeWitt I, Rauschecker JP (2012) Phoneme and word recognition in the auditory ventral stream. *Proc Natl Acad Sci USA* 109(8):E505–E514.

22. Beaulieu C (2002) The basis of anisotropic water diffusion in the nervous system—A technical review. *NMR Biomed* 15(7-8):435–455.
23. de Diego Balaguer R, Toro JM, Rodriguez-Fornells A, Bachoud-Lévi A-C (2007) Different neurophysiological mechanisms underlying word and rule extraction from speech. *PLoS ONE* 2(11):e1175.
24. MacMillan N, Creelman C (2005) *Detection Theory: A User's Guide.* (Lawrence Elbaum, Mahwah, NJ) 2nd ed.
25. Chevillet MA, Jiang X, Rauschecker JP, Riesenhuber M (2013) Automatic phoneme category selectivity in the dorsal auditory stream. *J Neurosci* 33(12):5208–5215.
26. Buchsbaum BR, D'Esposito M (2008) The search for the phonological store: From loop to convolution. *J Cogn Neurosci* 20(5):762–778.
27. Cunillera T, et al. (2009) Time course and functional neuroanatomy of speech segmentation in adults. *Neuroimage* 48(3):541–553.
28. Romanski LM, Tian B, Fritz J, Mishkin M, Rauschecker JP (1999) Dual streams of auditory afferents target multiple domains in the primate prefrontal cortex. *Nat Neurosci* 2(12):1131–1136.
29. Mestres-Missé A, Càmara E, Rodríguez-Fornells A, Rotte M, Münte TF (2008) Functional neuroanatomy of meaning acquisition from context. *J Cogn Neurosci* 20(12): 2153–2166.
30. Catani M, et al. (2013) A novel frontal pathway underlies verbal fluency in primary progressive aphasia. *Brain*, 10.1093/brain/awt163.
31. Geschwind N (1970) The organization of language and the brain. *Science* 170(3961): 940–944.
32. Johnson SC, Saykin AJ, Flashman LA, McAllister TW, Sparling MB (2001) Brain activation on fMRI and verbal memory ability: Functional neuroanatomic correlates of CVLT performance. *J Int Neuropsychol Soc* 7(1):55–62.
33. Stein M, et al. (2012) Structural plasticity in the language system related to increased second language proficiency. *Cortex* 48(4):458–465.
34. Golestani N, Price CJ, Scott SK (2011) Born with an ear for dialects? Structural plasticity in the expert phonetician brain. *J Neurosci* 31(11):4213–4220.
35. Golestani N, Paus T, Zatorre RJ (2002) Anatomical correlates of learning novel speech sounds. *Neuron* 35(5):997–1010.
36. Golestani N, Molko N, Dehaene S, LeBihan D, Pallier C (2007) Brain structure predicts the learning of foreign speech sounds. *Cereb Cortex* 17(3):575–582.
37. Mårtensson J, et al. (2012) Growth of language-related brain areas after foreign language learning. *Neuroimage* 63(1):240–244.
38. Lee H, et al. (2007) Anatomical traces of vocabulary acquisition in the adolescent brain. *J Neurosci* 27(5):1184–1189.
39. Mechelli A, et al. (2004) Structural plasticity in the biligual brain. *Nature* 431:757.
40. Fields RD (2008) White matter in learning, cognition and psychiatric disorders. *Trends Neurosci* 31(7):361–370.
41. Beaulieu C (2010) *Diffusion MRI*, ed Jones DK (Oxford Univ Press, New York), pp 92–109.
42. Song S-K, et al. (2002) Dysmyelination revealed through MRI as increased radial (but unchanged axial) diffusion of water. *Neuroimage* 17(3):1429–1436.
43. Ogawa S, Lee TM (1990) Magnetic resonance imaging of blood vessels at high fields: In vivo and in vitro measurements and image simulation. *Magn Reson Med* 16(1):9–18.
44. Kwong KK, et al. (1992) Dynamic magnetic resonance imaging of human brain activity during primary sensory stimulation. *Proc Natl Acad Sci USA* 89(12):5675–5679.
45. Logothetis NK, Pauls J, Augath M, Trinath T, Oeltermann A (2001) Neurophysiological investigation of the basis of the fMRI signal. *Nature* 412(6843):150–157.
46. Ogawa S, Lee TM, Nayak AS, Glynn P (1990) Oxygenation-sensitive contrast in magnetic resonance image of rodent brain at high magnetic fields. *Magn Reson Med* 14(1):68–78.
47. Demerens C, et al. (1996) Induction of myelination in the central nervous system by electrical activity. *Proc Natl Acad Sci USA* 93(18):9887–9892.
48. Zatorre RJ, Fields RD, Johansen-Berg H (2012) Plasticity in gray and white: Neuroimaging changes in brain structure during learning. *Nat Neurosci* 15(4):528–536.
49. Petrides M, Pandya DN (2009) Distinct parietal and temporal pathways to the homologues of Broca's area in the monkey. *PLoS Biol* 7(8):e1000170.
50. Schenker NM, et al. (2008) A comparative quantitative analysis of cytoarchitecture and minicolumnar organization in Broca's area in humans and great apes. *J Comp Neurol* 510(1):117–128.
51. Rilling JK, Glasser MF, Jbabdi S, Andersson J, Preuss TM (2011) Continuity, divergence, and the evolution of brain language pathways. *Front Evol Neurosci* 3:11.
52. Fritz J, Mishkin M, Saunders RC (2005) In search of an auditory engram. *Proc Natl Acad Sci USA* 102(26):9359–9364.
53. Brauer J, Anwander A, Friederici AD (2011) Neuroanatomical prerequisites for language functions in the maturing brain. *Cereb Cortex* 21(2):459–466.
54. Brauer J, Anwander A, Perani D, Friederici AD (2013) Dorsal and ventral pathways in language development. *Brain Lang*, 10.1016/j.bandl.2013.03.001.
55. Yeatman JD, Feldman HM (2013) Neural plasticity after pre-linguistic injury to the arcuate and superior longitudinal fasciculi. *Cortex* 49(1):301–311.
56. Rauschecker AM, et al. (2009) Reading impairment in a patient with missing arcuate fasciculus. *Neuropsychologia* 47(1):180–194.
57. Dell'Acqua F, Catani M (2012) Structural human brain networks: Hot topics in diffusion tractography. *Curr Opin Neurol* 25(4):375–383.
58. Catani M, Thiebaut de Schotten M, Slater D, Dell'Acqua F (2013) Connectomic approaches before the connectome. *Neuroimage*, 10.1016/j.neuroimage.2013.05.109.
59. Johansen-Berg H (2007) Structural plasticity: Rewiring the brain. *Curr Biol* 17(4): R141–R144.
60. Oldfield RC (1971) The assessment and analysis of handedness: The Edinburgh inventory. *Neuropsychologia* 9(1):97–113.
61. Dutoit T, Pagel V, Pierret N, Bataille F, Vrecken O (1996) The MBROLA project: Towards a set of high-quality speech synthesizers free of use for non-commercial purposes. *Proceedings of The Fourth International Conference on Spoken Language Processing '96* (3) (Philadephia), pp 1393–1396.
62. Peña M, Bonatti LL, Nespor M, Mehler J (2002) Signal-driven computations in speech processing. *Science* 298(5593):604–607.
63. Leemans A, Jones DK (2009) The B-matrix must be rotated when correcting for subject motion in DTI data. *Magn Reson Med* 61(6):1336–1349.
64. Chang L-C, Jones DK, Pierpaoli C (2005) RESTORE: Robust estimation of tensors by outlier rejection. *Magn Reson Med* 53(5):1088–1095.
65. Jones DK, Basser PJ (2004) "Squashing peanuts and smashing pumpkins": How noise distorts diffusion-weighted MR data. *Magn Reson Med* 52(5):979–993.
66. Basser PJ, Pajevic S, Pierpaoli C, Duda J, Aldroubi A (2000) In vivo fiber tractography using DT-MRI data. *Magn Reson Med* 44(4):625–632.
67. Wang R, Benner T, Sorensen A, Wedeen V (2007) Diffusion toolkit: A software package for diffusion imaging data processing and tractography. *Proceedings of the International Society for Magnetic Resonance in Medicine* (Berlin), p 3720.
68. Catani M, Thiebaut de Schotten M (2008) A diffusion tensor imaging tractography atlas for virtual in vivo dissections. *Cortex* 44(8):1105–1132.
69. Klawiter EC, et al. (2011) Radial diffusivity predicts demyelination in ex vivo multiple sclerosis spinal cords. *Neuroimage* 55(4):1454–1460.
70. Naismith RT, et al. (2010) Radial diffusivity in remote optic neuritis discriminates visual outcomes. *Neurology* 74(21):1702–1710.
71. Ashburner J (2007) A fast diffeomorphic image registration algorithm. *Neuroimage* 38(1):95–113.
72. Zhou D, Thompson WK, Siegle G (2009) MATLAB toolbox for functional connectivity. *Neuroimage* 47(4):1590–1607.
73. Barber AD, et al. (2012) Motor "dexterity"?: Evidence that left hemisphere lateralization of motor circuit connectivity is associated with better motor performance in children. *Cereb Cortex* 22(1):51–59.

Supporting Information

López-Barroso et al. 10.1073/pnas.1301696110

SI Materials and Methods

Regions of Interest for Virtual Dissections. ***Tractography of the arcuate fasciculus.*** A two-regions of interest (ROI) approach was defined to encompass the streamlines of the arcuate fasciculus (AF), allowing us to differentiate the direct (long) from the indirect (anterior and posterior) segments. This approach has been previously described (1, 2). First, to dissect the long segment, located medially with respect to the indirect segments, two ROIs were created in the frontal and the posterior temporal cortices. To draw the frontal ROI, an area was defined on a coronal slice anterior to the central sulcus, where fibers of the AF are colored in green (indicating anterior-posterior orientation) in the color fiber-orientation map. The temporal ROI was defined on an axial slice through the posterior portion of the temporal stem; the voxels contained by this ROI appeared as blue, indicating dorsal-ventral orientation of the underlying fibres. All streamlines passing through these frontal and temporal ROIs were attributed to the long direct segment of the AF and were labeled in red for display purposes (Fig. 1*B*). To dissect both the anterior and the posterior indirect segments, constituting both the lateral indirect pathway of the arcuate, a third ROI was selected in the inferior parietal region (Geschwind's territory). This ROI was defined on a sagittal slice around the borders of the angular and supramarginal gyrus. All streamlines passing through the frontal and parietal ROIs were attributed to the anterior indirect segment and those passing through the parietal and the temporal ROIs were considered to belong to the posterior indirect segment. Anterior and posterior segments were colored in green and yellow, respectively, for display purposes (Fig. 1*B*). The same approach was repeated for the right hemisphere.

Tractography dissections of the inferior fronto-occipital fasciculus. To dissect the inferior fronto-occipital fasciculus (IFOF), two spheres of 7 mm were used. The first sphere was located in the white matter of a posterior region located between the occipital and the temporal lobe. The second sphere was located on the white matter of the anterior floor of the external/extreme capsule, encompassing the fibers running from the temporal to the frontal lobe (3). Fig. S1 shows an example of the IFOF in one subject.

ROIs for Functional Analysis. Three large ROIs were manually drawn on the left and right hemispheres over the normalized mean structural T1 template from all participants using MRICRON software (4). The ROIs were drawn on consecutive slices following a lateral to medial direction (Fig. S3). The frontal ROI (covering Broca's territory), which encompasses the posterior part of the inferior frontal and middle frontal gyri and the premotor cortex, was drawn around the dorsolateral and ventrolateral prefrontal cortex anterior to the inferior and superior precentral sulcus. The temporal ROI (covering Wernicke's territory) encompasses the posterior part of the superior and middle temporal gyri and was drawn from the primary auditory cortex to the posterior part of the temporal cortex, covering both the middle and the superior temporal gyrus. The parietal ROI (covering Geschwind's territory) included both supramarginal and angular gyri in the inferior parietal lobe (Fig. S3).

As the ROIs were defined manually, we needed to control for the amount of white matter in each region. A ROI including mostly white matter might not show the most important functional peaks (which would be restricted to gray matter), leading to biased functional connectivity results. To calculate the amount of gray matter and white matter inside each anatomical ROI, the group gray matter and white matter templates calculated during DARTEL normalization (see *Materials and Methods*) were used. By overlapping each of the ROIs, which were depicted using the normalized mean structural T1 template, with the mean gray matter and white matter templates, the amount of each tissue inside of each anatomical ROI was estimated. Two measures, percentage of tissue overlap and the Dice Similarity Index were extracted (DSI) (5). Percentage of tissue overlap was defined as the percentage of gray matter or white matter volume inside the anatomical ROI ($V_{GM/WM}$ * $100/V_{ROI}$). DSI ranges between 0 and 1 (0 indicating no overlap and 1 indicating a perfect similarity) and takes into account both false negatives and false positives. In this case, the DSI was defined as twice the overlap between the volume of gray matter or white matter and the volume of the anatomical ROI, divided by the total volume sum $\left(\frac{2*\left(V_{GM/WM}\cap\ V_{ROI}\right)}{V_{GM/WM}+V_{ROI}}\right)$. DSI values between 0.6 and 0.8 have been regarded as an indicator of good overlap, and values exceeding 0.8 are considered excellent (6, 7). Results are shown in Table S6.

Both measures of overlap show clearly that gray matter is the predominant tissue in each of the ROIs, constituting around 65% of the brain tissue inside each anatomical ROI and yielding an extremely high DSI (around 0.80). On the other hand, it is important to note that for the functional connectivity analysis, the mean blood oxygen level-dependent (BOLD) response was extracted from an 8-mm radius seed around each subject's specific peak maxima inside each of the anatomical ROIs. Thus, taking together that most of the anatomical ROIs are constituted of gray matter and that the BOLD signal was extracted from the mean response of all of the voxels inside an 8-mm radius seed, the possibility of white matter voxels tampering with the functional connectivity analysis is low.

Behavioral Performance: *d′* Analysis. To obtain a measurement of the participants' performance in the word learning test without response bias (e.g., the trend to answer "Yes" in all of the trials, resulting in a 50% of hits), their behavioral responses were transformed to *d*-prime (*d′*) (8). *d′* reflects an individual's ability to distinguish true signals (presented words) from noise (nonpresented words). For each participant, the proportion of hits (i.e., previously presented word correctly identified) and false alarms (i.e., nonpresented words identified as previously presented) were used to calculate a *d′* score. Then, a one-sample *t* test against 0 (*d′* = 0 corresponds to no discrimination) was performed to evaluate if participants were able to discriminate words presented in the artificial language from nonwords.

Lateralization analysis.

Tractography. Individual dissections of each of the three segments of the AF in both hemispheres suggested an asymmetrical pattern of distribution (Fig. S2*A*). To confirm this finding, the lateralization index for each segment—long, anterior, and posterior—was calculated for the number of streamlines and the fractional anisotropy (FA). The lateralization index has been used in previous studies to assess microstructural differences in WM structures between hemispheres (2, 9). The lateralization index ranges between −1 and 1, where negative values represent right lateralization, values around zero represent symmterical distribution, and positive values a left lateralization. A one-sample *t* test (test value = 0) was used to assess the significance of the lateralization for the three arcuate segments and the IFOF. For the number of streamlines, two segments of the AF showed

a clear pattern of lateralization: the long segment showed a left lateralization (Fig. S2*B*, red dots, and Table S2) and the anterior segment showed a right lateralization (Fig. S2*B*, green dots, and Table S2). The posterior segment showed a symmetrical distribution (Fig. S2*B*, yellow dots, and Table S2). After removing an outlier, the anterior segments showed greater right lateralization [$n = 20$, mean lateralization index: -0.42, $t(19) = -4.8$, $P < 0.0001$]. Twenty-five percent of our sample showed an extreme left lateralization of the long segment. This pattern of lateralization, showing a left lateralization of the long segment, a right lateralization of the anterior segment, and a symmetrical distribution of the posterior segment, replicates previous results in healthy adult subjects (2). Similarly, lateralization analysis was calculated for the FA. A rightward distribution of the anterior segment was found (Table S2). Finally, lateralization analysis of the IFOF indicated a symmterical distribution in the number of streamlines (Fig. S2, blue dots), with a left lateralization for the FA (Table S2).

Functional connectivity. To explore a possible relationship between learning scores and functional lateralization, the lateralized difference in hemispheric connectivity was calculated (10). This was done by simply subtracting, for each subject, the left *z*-transformed correlation minus the right *z*-transformed correlation (Left Hemisphere-Right Hemisphere) for each pair of regions connected by the direct and the indirect segments of the AF (Broca-Wernicke, Broca-Geschwind, Geschwind-Wernicke).

Functional MRI main contrast of interest. Distinct brain regions, covering motor and auditory areas, including the bilateral superior temporal and posterior superior temporal cortex, bilateral premotor cortex, and left inferior frontal gyrus, showed significant activation in the language versus baseline second-level group contrast at a $P < 0.05$, false-discovery rate (FDR)-corrected threshold (Fig. 3*B* and Table S5), replicating previous functional MRI findings (11, 12).

1. Catani M, Jones DK, ffytche DH (2005) Perisylvian language networks of the human brain. *Ann Neurol* 57(1):8–16.
2. Catani M, et al. (2007) Symmetries in human brain language pathways correlate with verbal recall. *Proc Natl Acad Sci USA* 104(43):17163–17168.
3. Catani M, Thiebaut de Schotten M (2008) A diffusion tensor imaging tractography atlas for virtual in vivo dissections. *Cortex* 44(8):1105–1132.
4. Rorden C, Brett M (2000) Stereotaxic display of brain lesions. *Behav Neurol* 12(4):191–200.
5. Dice L (1945) Measures of the amount of ecologic association between species. *Ecology* 26:297–302.
6. Ripollés P, et al. (2012) Analysis of automated methods for spatial normalization of lesioned brains. *Neuroimage* 60(2):1296–1306.
7. Wilke M, de Haan B, Juenger H, Karnath H-O (2011) Manual, semi-automated, and automated delineation of chronic brain lesions: A comparison of methods. *Neuroimage* 56(4):2038–2046.
8. MacMillan N, Creelman C (2005) *Detection Theory: A User's Guide.* (Lawrence Elbaum, Mahwah, NJ) 2nd ed.
9. Thiebaut de Schotten M, et al. (2011) A lateralized brain network for visuospatial attention. *Nat Neurosci* 14(10):1245–1246.
10. Barber AD, et al. (2012) Motor "dexterity"?: Evidence that left hemisphere lateralization of motor circuit connectivity is associated with better motor performance in children. *Cereb Cortex* 22(1):51–59.
11. Cunillera T, et al. (2009) Time course and functional neuroanatomy of speech segmentation in adults. *Neuroimage* 48(3):541–553.
12. McNealy K, Mazziotta JC, Dapretto M (2006) Cracking the language code: Neural mechanisms underlying speech parsing. *J Neurosci* 26(29):7629–7639.

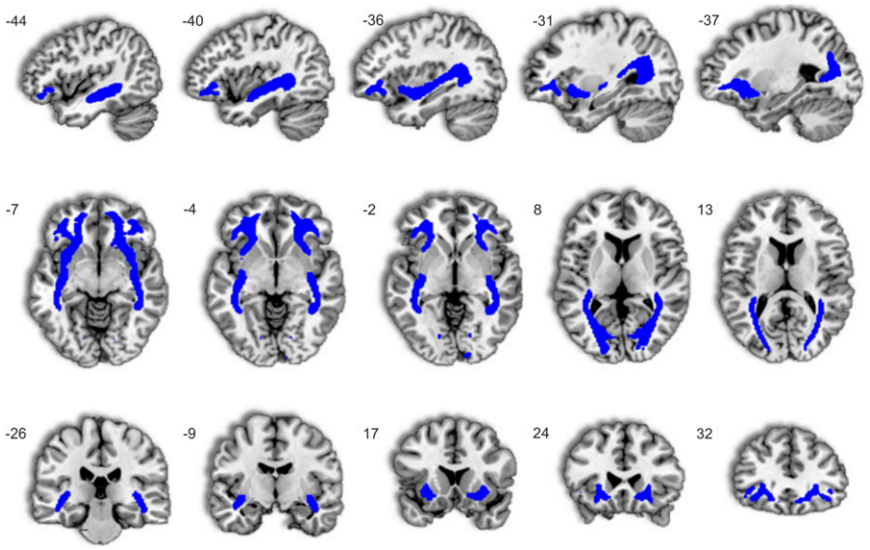

Fig. S1. Bilateral reconstruction of the IFOF from one representative subject normalized to Montreal Neurological Institute (MNI) 152 space and overlaid on a MNI template (chbet) provided in MRICRON (4). Neurological convention is used (left is left). On the top row, only the left hemisphere is shown. On the top left of each slice, the MNI coordinate is shown.

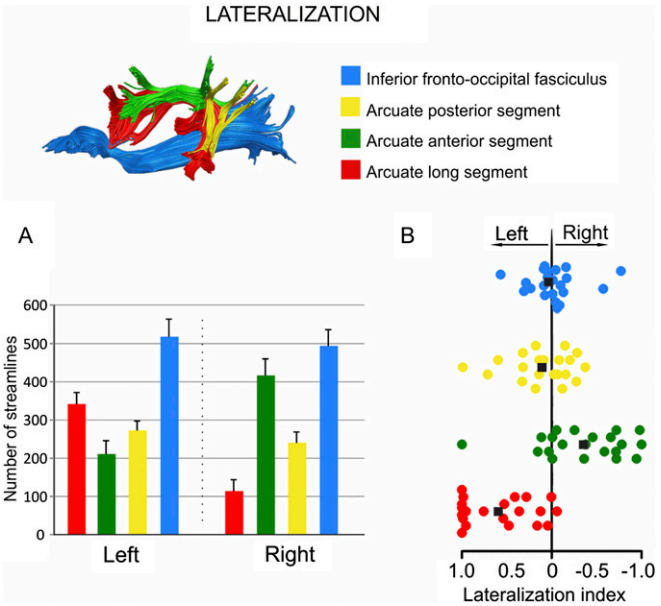

Fig. S2. Distribution of the number of streamlines of the AF and IFOF between hemispheres. (*A*) Average number (and standard deviation) of the streamlines for each pathway in each hemisphere. (*B*) Lateralization index show that the long arcuate segment (red) was significantly left lateralized while the anterior indirect segment (green) showed a right lateralization. Both posterior indirect AF segment (yellow) and IFOF (blue) showed a symmetrical distribution. The black square indicates the mean lateralization index (number of streamlines) for each pathway.

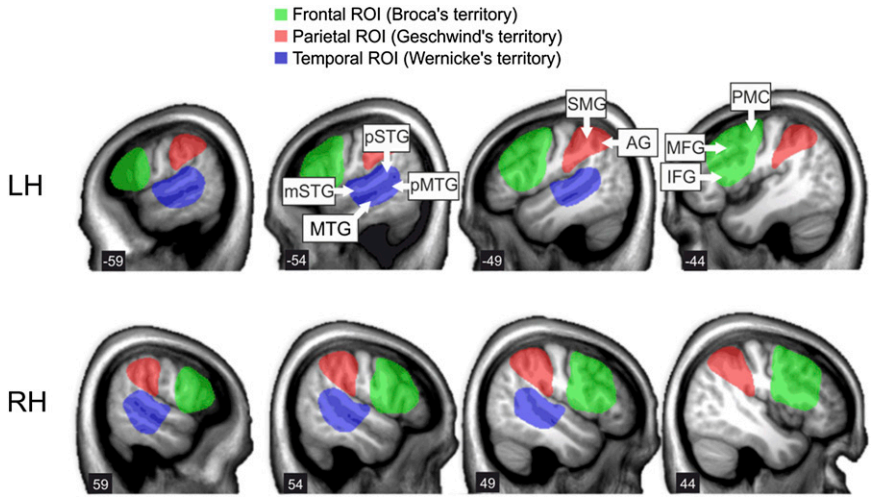

Fig. S3. An illustration of the three ROIs used for functional connectivity analysis. MNI coordinates are shown in the left bottom corner of each slide. AG, angular gyrus; IFG, inferior frontal gyrus; LH, left hemisphere; MFG, middle frontal gyrus; MTG, middle temporal gyrus; mSTG, middle superior temporal gyrus; PMC, premotor cortex; pMTG, posterior middle temporal gyrus; pSTG, posterior superior temporal gyrus; RH, right hemisphere; SMG, supramarginal gyrus.

Table S1. Correlations between each segment of the AF and word learning performance

Segment	Value type	NS	FA	RD
Left				
Long	*r*	0.22	0.48	−0.6
	P	n.s.	0.031	0.005*
	n	20	20	20
Anterior	*r*	0.17	0.20	−0.2
	P	n.s.	n.s.	n.s.
	n	20	19	19
Posterior	*r*	0.11	0.19	−0.42
	P	n.s.	n.s.	n.s.
	n	19	19	19
Right				
Long	*r*	−0.24	0.18	−0.44
	P	n.s.	n.s.	n.s.
	n	20	15	15
Anterior	*r*	0.1	0.2	−0.32
	P	n.s.	n.s.	n.s.
	n	19	18	18
Posterior	*r*	0.23	0.04	-0.42
	P	n.s.	n.s.	n.s.
	n	19	19	19

Correlations were performed for number of streamlines (NS), fractional anisotropy (FA) and radial diffusivity (RD); n.s., not significant. An asterisk marks the correlations that survived the Bonferroni's correction for multiple comparisons.

Table S2. Lateralization index for each pathway and correlations with word learning scores

	LI		Correlation with learning scores		
Pathway	Ns	FA	Value	Ns	FA
Long AF	0.59**	0.01	*r*	0.28	0.05
			P	n.s.	n.s.
			n	20	15
Anterior AF	−0.35*	−0.02*	*r*	0.11	−0.31
			P	n.s.	n.s.
			n	20	18
Posterior AF	0.11	−0.004	*r*	−0.17	0.1
			P	n.s.	n.s.
			n	20	20
IFOF	0.026	0.011**	*r*	−0.09	0.25
			P	n.s.	n.s.
			n	20	20

LI ranges from 1 to −1, where positive values indicate a leftward asymmetry and negative values indicate a rightward asymmetry. AF, arcuate fasciculus; FA, fractional anisotropy; IFOF, inferior occipito-frontal fasciculus; LI, lateralization index; Ns, number of streamlines; n.s., not significant. *$P < 0.005$; **$P < 0.0001$.

Table S3. Correlation indexes between the microstructure of the IFOF and the word learning scores

Pathway	Value	NS	FA	RD
Left IFOF	*r*	0.07	0.34	−0.45
	P	n.s.	n.s.	0.04
	n	20	20	20
Right IFOF	*r*	0.06	0.23	−0.30
	P	n.s.	n.s.	n.s.
	n	20	20	20

Correlations were performed for different surrogate DTI measures of volume and white matter miscrostructure: FA, fractional anisotropy; IFOF, inferior fronto-occipital fasciculus; NS, number of streamlines; n.s., not significant; RD, radial diffusivity. None of the correlations survived Bonferroni's correction for multiple comparisons.

Table S4. Correlations between the functional connectivity laterality index of each pair of regions and word learning performance

Pairs of regions	*P* and *r* values
Broca–Wernicke	$r = 0.28$
	$P > 0.16$
Broca–Geschwind	$r = -0.34$
	$P > 0.09$
Geschwind–Wernicke	$r = 0.02$
	$P > 0.90$

Table S5. Main areas of activation for the language vs. baseline contrast at the group level with a $P < 0.05$ FDR-corrected threshold

Activation region	MNI coordinates	Cluster size (no. of voxels)	*t* value (FDR *P* value)
Right superior temporal gyrus	57 −17 6	10,803	18.89 (0.001)
Left superior temporal gyrus	−42 −30 8	10,395	16.47 (0.001)
Left precentral gyrus	−51 −6 45	944	7.33 (0.001)
Right precentral gyrus	54 −3 48	1,043	5.91(0.015)
Left supplementary motor area	−3 3 63	522	5.81 (0.015)
Left inferior frontal gyrus (pars triangularis)	−48 15 27	939	4.85 (0.047)

Table S6. Percentage of tissue overlap and Dice Similarity Index for each ROI and tissue

GM/WM	Left Broca	Right Broca	Left Wernicke	Right Wernicke	Left Geschwind	Left Geschwind
Percentage of tissue overlap						
GM	64.05	64.21	68.48	66.03	66.44	69.29
WM	32.84	33.53	29.85	32.65	24.52	26.29
Dice similarity index						
GM	0.78	0.78	0.81	0.80	0.80	0.82
WM	0.49	0.50	0.46	0.49	0.39	0.42